CrossMark

ORIGINAL RESEARCH

An investigation of structural and magnetic properties of Cr–Zn ferrite nanoparticles prepared by a sol–gel process

M. Lakshmi[1] · K. Vijaya Kumar[2] · K. Thyagarajan[3]

Abstract Cr_x Zn Fe_{2-x} O_4 (with $x = 0.0$, 0.1, 0.2, 0.3, 0.4, and 0.5) spinel ferrite nanoparticles have been synthesized via sol–gel method. The precursor compound was calcined at a temperature of 900 °C for 3 h. The aim of this study was to investigate the effect of Cr^{3+} ion substitution on the structural and magnetic properties of Cr–Zn ferrite. The size, shape, and chemical state of the synthesized powders were structurally characterized by powder XRD, SEM, TEM, HRTEM, SAED, energy-dispersive X-ray analysis (EDAX), and Fourier transform infrared spectroscopy (FTIR) spectral techniques. The XRD pattern of Cr–Zn ferrite provides information about single-phase formation of spinel structure with cubic symmetry. Both crystallite size and lattice parameter decrease with increasing Cr content. Formation of spinel structure is affirmed by using FTIR and FTIR spectra which shows that the bands $\upsilon 1$ and $\upsilon 2$ are found to shift gradually toward the higher frequency side with substitution of Cr, which have been attributed to the decrease in the lattice constant. SEM and TEM micrographs demonstrated that nanoparticles with narrow size distribution were obtained. The average grain size was found to be in nanometer range and of the order of 43–63 nm obtained using TEM images. Compositional stoichiometry was confirmed by EDAX technique. The magnetic properties of synthesized chromium-substituted Zn ferrite nanoparticles were studied using vibrating sample magnetometer at room temperature under the applied magnetic field of 15 KG. The result indicated that the amount of Cr contents significantly influenced the crystal morphology and structural and magnetic properties of Cr-doped Zn ferrite nanoparticles.

Keywords Sol–gel · Spinel ferrite · XRD · FTIR · SEM · TEM · Magnetic properties

Introduction

Magnetic materials, particularly nano-sized ferrites, show a significant change in physical, electrical, and magnetic properties in contrast to their bulk counterparts due to their high surface-to-volume ratio of the grains. Ferrite nanoparticles have scientific and technological importance in recent years due to their magnetic properties and wide range of applications especially when the size of the particles approaches to nanometer scale [1]. They have been used for high-frequency transformer cores, rod antennas, and radio-frequency coils [2, 3]. More recently, these are also used in nano-electronic devices, high-speed integrated circuits as well as in biomedical field as contrasting agents used for magnetic resonance imaging (MRI) [4–7]. Spinel ferrites are materials with good magnetic and electronic properties, which depend strongly on the cation distribution among the tetrahedral and octahedral sites [8]. Among the spinel ferrites, nanoparticles of Zinc ferrite ($ZnFe_2O_4$) are the potential candidate for various applications such as radar-absorbing materials, gas sensors, photo-catalyst, and

✉ K. Vijaya Kumar
drkvk1974@gmail.com

1 Marri Laxman Reddy Institute of Technology and Management, Dundigal, Quthbullapur Mandal, Hyderabad 500043, TS, India

2 Department of Physics, Jawaharlal Nehru Technological University Hyderabad College of Engineering Jagtial, Nachupally (Kondagattu), Karimnagar – Dist. 505501, TS, India

3 Department of Physics, Jawaharlal Nehru Technological University Anantapur College of Engineering, Pulivendula, YSR – Dist. 516390, AP, India

Springer

electromagnetic wave-absorbing materials [9, 10]. Preparation method and chemical composition play a key role in incurring ferrites with high quality. Sol–gel method is the most useful and attractive technique for the fabrication of ferrite nanoparticles due to its advantages like good stoichiometric control, the possibility of obtaining ultra-fine particles in the nano-regime with high crystallinity, superior purity, and uniform particle distribution in a relatively short processing time at a very low temperature with simple laboratory equipment [6, 11]. The present study is focused on the synthesis of Zn ferrite by doping with Cr^{3+} ions to explore their applicability in nano-devices. Thus with appropriate selection of preparation method and precursors (metal nitrates) single-phase cubic spinel structure Cr–Zn ferrite nanoparticles with enhanced structural and magnetic properties have been fabricated.

Experimental details

Synthesis of Cr–Zn ferrites

Cr-substituted Zn ferrite with a chemical formula $Cr_x Zn Fe_{2-x} O_4$ (where, $x = 0.0, 0.1, 0.2, 0.3, 0.4,$ and 0.5) have been synthesized through sol–gel method. The analytical-grade $Fe(NO_3)_3.9H_2O$, $Zn(NO_3)_2 .6H_2O$, $Cr(NO_3)_3.9H_2O$ and $C_6H_8O_7.H_2O$ (Hydrated citric acid) were used as precursor materials. The weighed amounts of these metal nitrates were completely dissolved in small quantity of distilled water. This solution was then added to citric acid in such a way that in the final sample the molar ratio of these nitrates and citric acid becomes 1:1. A small amount of ammonia was drop-wise added to achieve a pH value of 7 for the solution with stirring it simultaneously. The solution is continuously stirred using a magnetic stirrer. Condensation reaction occurs between the adjacent metal nitrates and the molecules of citrates yielding a polymer network in colloidal dimensions known as sol. The stirring is continued for 1 h. The solution was evaporated by intensive stirring and heating for 1 h at 80 °C and was kept at this temperature until the sol turned into a gel. The gel was then heated at 180 °C for auto-combustion to take place. The dried gel was burnt in a self-propagating combustion manner until all the gel was burnt out completely to form loose powder. The resulting powder is crushed in an agate mortar to obtain the nanoferrites [12, 13]. The as-prepared ferrite powder was sintered at 900 °C for 3 h.

Characterization

X-ray diffraction (XRD) investigation was performed at room temperature using CuKα radiation of wavelength 1.5406 Å to confirm the crystallographic phase formation of $Cr_x Zn Fe_{2-x} O_4$ nanocrystalline ferrite material. The Fourier transform infrared (FTIR) spectra of the obtained powders were recorded using FTIR spectrometer in the wave number range 4000–400 cm^{-1} using KBr pellets to ratify the spinel structure of the samples. The surface morphology of the ferrite samples was examined using scanning electron microscopy (SEM). The microstructure and elemental analysis of the product material was done using transmission electron microscopy (TEM) along with energy-dispersive X-ray analysis (EDAX). In order to evaluate the magnetic properties, vibrating sample magnetometer (VSM) analysis was done at room temperature with maximum applied magnetic field of 15 KG.

Results and discussion

X-ray diffraction (XRD) analysis

The phase and purity of the synthesized Cr–Zn ferrites were examined by X-ray diffraction patterns and are shown in Fig. 1a. These patterns of the samples suggest the formation of single-phase spinel structure with cubic symmetry. It is observed that the peaks become broad from the sample with Cr content $x = 0$ to $x = 0.5$ which indicates that the size of the particle decreases with the increase of Cr^{3+} ion concentration. According to the Scherrer's equation, with reduction of crystallite size the full width at half maximum (FWHM) parameter will be enhanced and results in the broadening of the diffraction peaks. The crystallite size is evaluated by measuring the FWHM of the most intense (311) peak from XRD pattern and by using the following Debye–Scherrer equation:

$$d = 0.9\lambda/\beta \cos\theta, \qquad (1)$$

where d is the crystallite size, 0.9 is the symmetry constant, λ is the wavelength of incident X-ray, θ is the diffraction angle, and β is the full width at half maximum (FWHM). The analysis revealed that the crystallite sizes are in the range of 24–34 nm and exhibit gradual decrease with the increasing Cr^{3+} content.

The interplanar spacing (d) values were calculated for the recorded peaks using Bragg's law:

$$n\lambda = 2d \sin\theta. \qquad (2)$$

The lattice constant (a) of individual sample was calculated using the following relationship:

$$a = d_{hkl}\left(\sqrt{h^2 + k^2 + l^2}\right), \qquad (3)$$

where $dhkl$ is the interplanar distance for hkl planes; the lattice constant 'a' was calculated for (311) plane and the lattice parameter was found to decrease with the increase of Cr^{3+} ions in the Cr–Zn spinel ferrites. Figure 1b represents
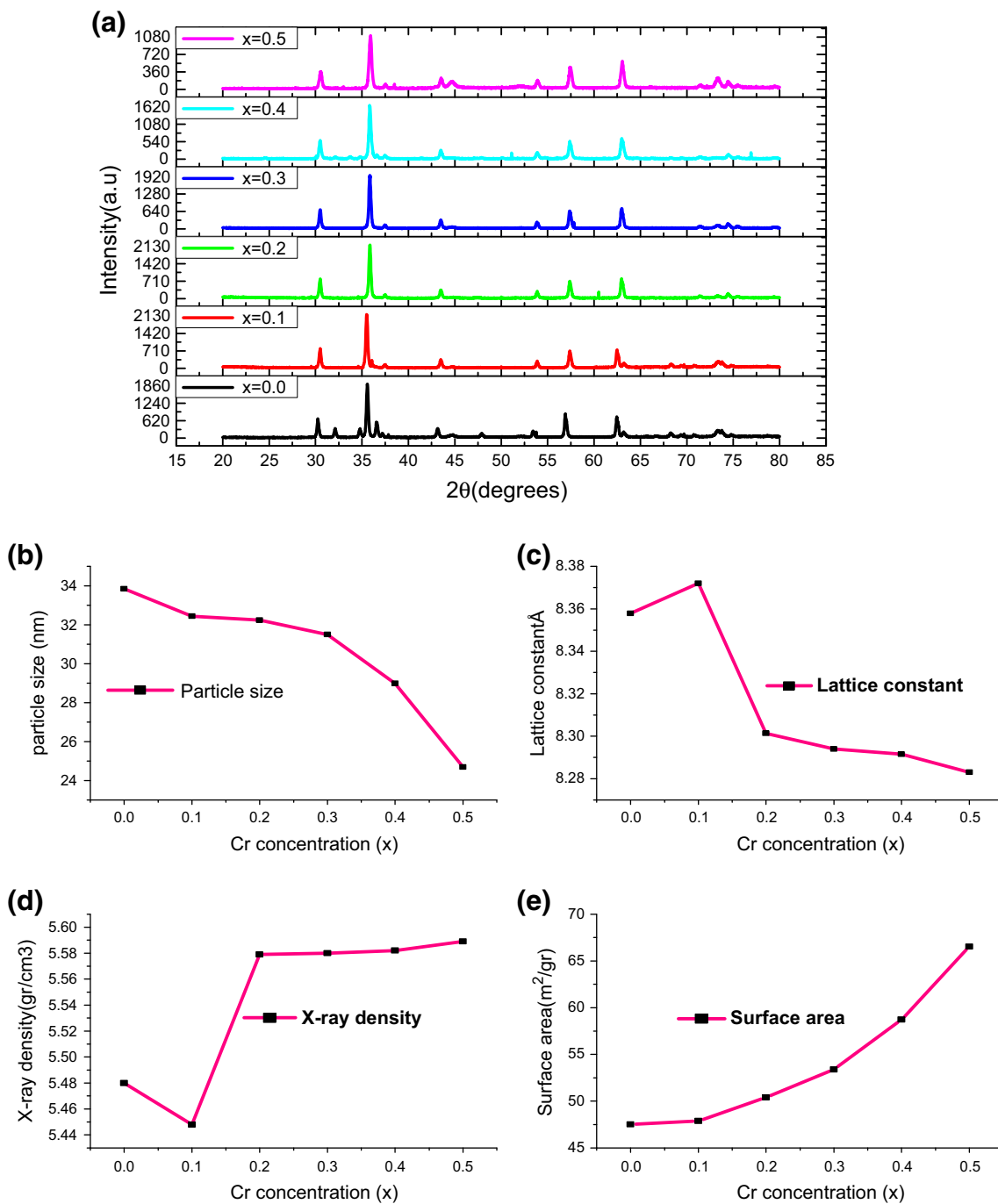
Fig. 1 The XRD patterns for Crx Zn Fe2−x O4 with x = 0.0, 0.1, 0.2, 0.3, 0.4, and 0.5. **b–e** The variation of structural parameters with Cr^{3+} content (x) for various Crx Zn Fe−x O4 samples

the variation of lattice constant with the Cr^{3+} ion concentration in the Zn ferrite samples. The decrement in the lattice parameter is attributed to the replacement of Fe^{3+} (0.67 Å) ion by Cr^{3+}, a smaller ion with the ionic radius of 0.64 Å [14, 15]. Similar behavior of lattice constant was reported in the literature [16].

X-ray density (ρ_x) of the prepared samples was measured using the following formula:

$$\rho_x = 8M/Na^3, \tag{4}$$

Table 1 Structural parameters of Cr_x Zn Fe_{2-x} O_4 ($x = 0.0$–0.5)

S. no	Cr content (x)	d (nm)	a (Å)	ρ_x (gr/cc)	ρ_b (gr/cc)	S (m²/gr)
1	$x = 0.0$	33.85	8.358	5.480	3.73	47.52
2	$x = 0.1$	32.43	8.372	5.448	3.864	47.88
3	$x = 0.2$	32.23	8.301	5.579	3.694	50.40
4	$x = 0.3$	31.50	8.294	5.580	3.567	53.40
5	$x = 0.4$	28.99	8.291	5.582	3.524	58.73
6	$x = 0.5$	24.69	8.283	5.589	3.652	66.54

where M is the molecular weight of the composition, N is the Avogadro's number (6.023×10^{23} atom/mole), and 'a' is the lattice constant. Bulk density (ρ_b) of the samples was calculated as

$$\rho_b = m/(\pi r^2 h), \tag{5}$$

where m, r, and h are mass, radius, and thickness of the pellet of sample, respectively. The ρ_x is inversely proportional to the lattice constant, which increases with increasing Cr^{+3} concentration. Density of polycrystalline ferrites plays a significant role in controlling the various properties. It is observed that the X-ray density (ρ_x) of each sample is greater than the corresponding bulk density (ρ_b). This may be due to some unavoidable pores created during sintering process [17].

The surface area (S) was determined using the following equation [18]:

$$S = \frac{6000}{(\rho_d)}, \tag{6}$$

where 'ρ' is the density and 'd' is the average particle size.

The particle size (d), lattice constant (a), bulk density (ρ_b), X-ray density (ρ_x), and surface area (S) are calculated using XRD reports. The calculated values are recorded in Table 1, and the dependence of the structural parameters on the concentration of substituted Cr^{3+} ion in Cr–Zn ferrite samples is depicted in Fig. 1b–e.

Using the values of lattice constant 'a,' the distance between magnetic ions (ion jump lengths) available in tetrahedral A-site and octahedral B-site, i.e., 'L_A' and 'L_B,' respectively, was calculated using the following relations [19]:

$$L_A = (\sqrt{3}/4)a \tag{7}$$

$$L_B = (\sqrt{2}/4)a. \tag{8}$$

Calculated values of ion jump lengths (L_A and L_B) are given in Table 2, which shows that ion jump lengths decreased with the increase in Cr concentration. Since lattice constant (a) is decreasing with the increases in Cr concentration (x), ion jump lengths (L_A and L_B) are directly proportional to lattice constant (a) value. Hence, ion jump lengths decreased with the increases in Cr concentration.

Table 2 Variation of hopping lengths (L_A and L_B) with Cr content x

S. no.	Cr content (x)	L_A (Å)	L_B (Å)
1	$x = 0.0$	3.619	2.954
2	$x = 0.1$	3.625	2.959
3	$x = 0.2$	3.595	2.935
4	$x = 0.3$	3.591	2.932
5	$x = 0.4$	3.590	2.931
6	$x = 0.5$	3.587	2.928

The variation in the ion jump lengths with respect to the Cr^{3+} concentration is depicted in Fig. 2.

Fourier transform infrared spectroscopy (FTIR) analysis

Fourier transformed infrared spectra of the investigated samples are shown in Fig. 3. Infrared spectroscopic study supported the formation of Cr–Zn spinel ferrite in the nanocrystalline form with enlightening two strong bands at around 600 and 400 cm^{-1} that are the common features of all spinel ferrites [20]. The typical bands of spinel structure are attributed to the stretching vibrations of the unit cell of the spinel in the tetrahedral (A) site and the metal–oxygen vibration in the octahedral (B) site [21]. These absorption bands are highly sensitive to changes in interaction between oxygen and cations, as well as to the size of the obtained nanoparticles [22]. The FTIR spectroscopic results are summarized in Table 3. The replacement of Fe^{3+} ions with Cr^{3+} ions at octahedral sites, which have smaller ionic radius and lower atomic mass, is the main reason for the observed shift in the $\upsilon2$ band position with increasing Cr concentration in the Zn ferrite. This behavior is in agreement with the observation noted by A.M.El. Sayed on Cr-doped Ni–Zn ferrites [23].

Scanning electron microscopy (SEM) analysis

Surface morphological properties of the chromium–zinc ferrite samples were studied using scanning electron microscopy (SEM). Figure 4a–e represents the SEM micrographs of Cr_x Zn Fe_{2-x} O_4 ($x = 0.1$–0.5) samples.

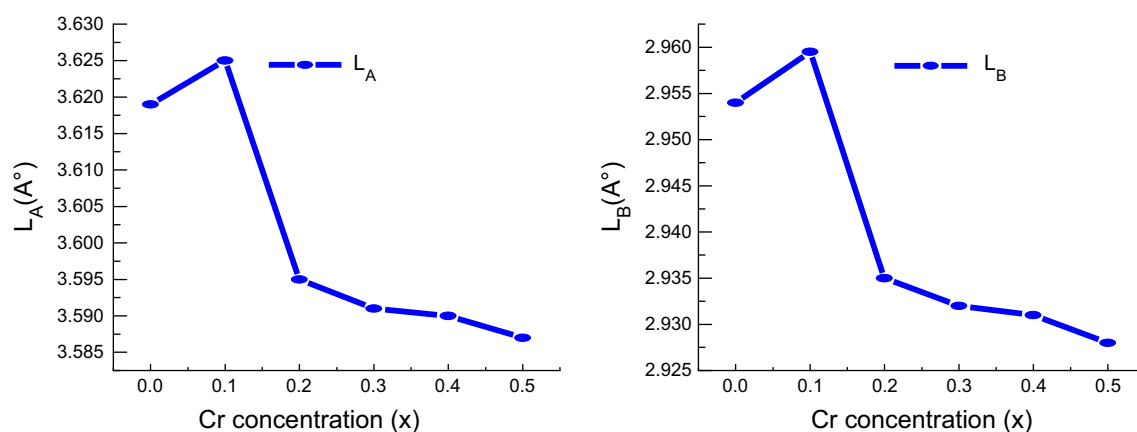**Fig. 2** The variation of hopping lengths with composition x

Fig. 3 FTIR spectra of Cr$_x$ Zn Fe$_{2-x}$ O$_4$ with $x = 0.0$(A1), 0.1(A2), 0.2(A3), 0.3(A4), 0.4(A5), and 0.5(A6)
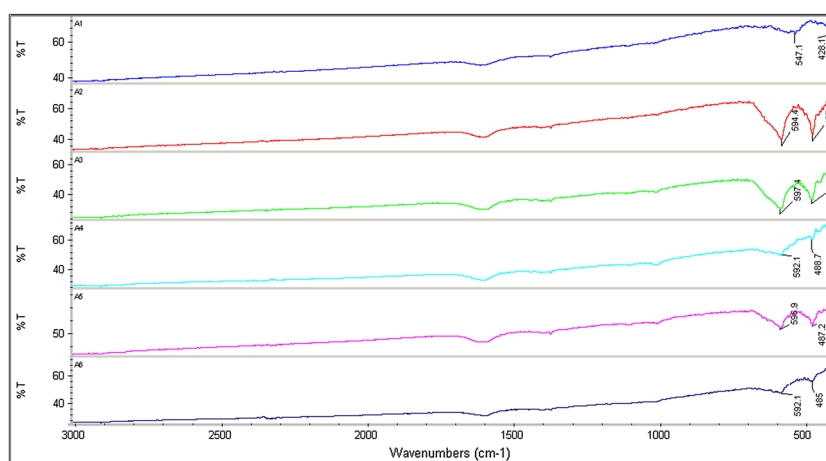
Table 3 Data on the position of FTIR absorption bands ($v1$, $v2$)

S. no	Cr content (x)	$v1$ (cm^{-1})	$v2$ (cm^{-1})
1	$x = 0.0$	547	428
2	$x = 0.1$	594	487
3	$x = 0.2$	597	490
4	$x = 0.3$	592	489
5	$x = 0.4$	596	487
6	$x = 0.5$	592	486

These micrographs show that the distribution of particles is uniform, and a close inspection would reveal the presence of particles showing cubic faces. SEM images clearly revealed that the particle size is decreasing with the increasing Cr concentration (x).

Transmission electron microscopy (TEM) analysis

Details about the structure, microstructure, and morphology of the obtained nanoparticles were provided by TEM studies. Figure 5a represents the TEM micrograph of Cr$_x$ Zn Fe$_{2-x}$ O$_4$ ($x = 0.3$) nanoparticles. TEM micrograph shows that the particles are formed in a controlled manner and the variation in the size of the particles is very small. The sizes of the nano-crystallites determined by TEM were in good agreement with the size calculated from peak broadening in X-ray diffraction pattern. Corresponding selected area electron diffraction (SAED) pattern (Fig. 5b) contains well-defined spotted rings indicating polycrystalline nature of the sample. As anticipated, the spotted appearance of the diffraction rings is due to high crystallinity of the obtained nanoparticles. Similar observation has also been reported earlier in the literature [24].

Usually High-resolution TEM (HRTEM) micrograph exhibits crystal lattice, as it is evident for a nanoparticles of incur ferrite sample. The HRTEM image of Cr–Zn ferrite ($x = 0.3$) nanoparticle is presented in Fig. 5c. The micrograph reveals highly ordered lattice fringes with a fringe separation of 2.53 Å, which corresponds to (311) lattice
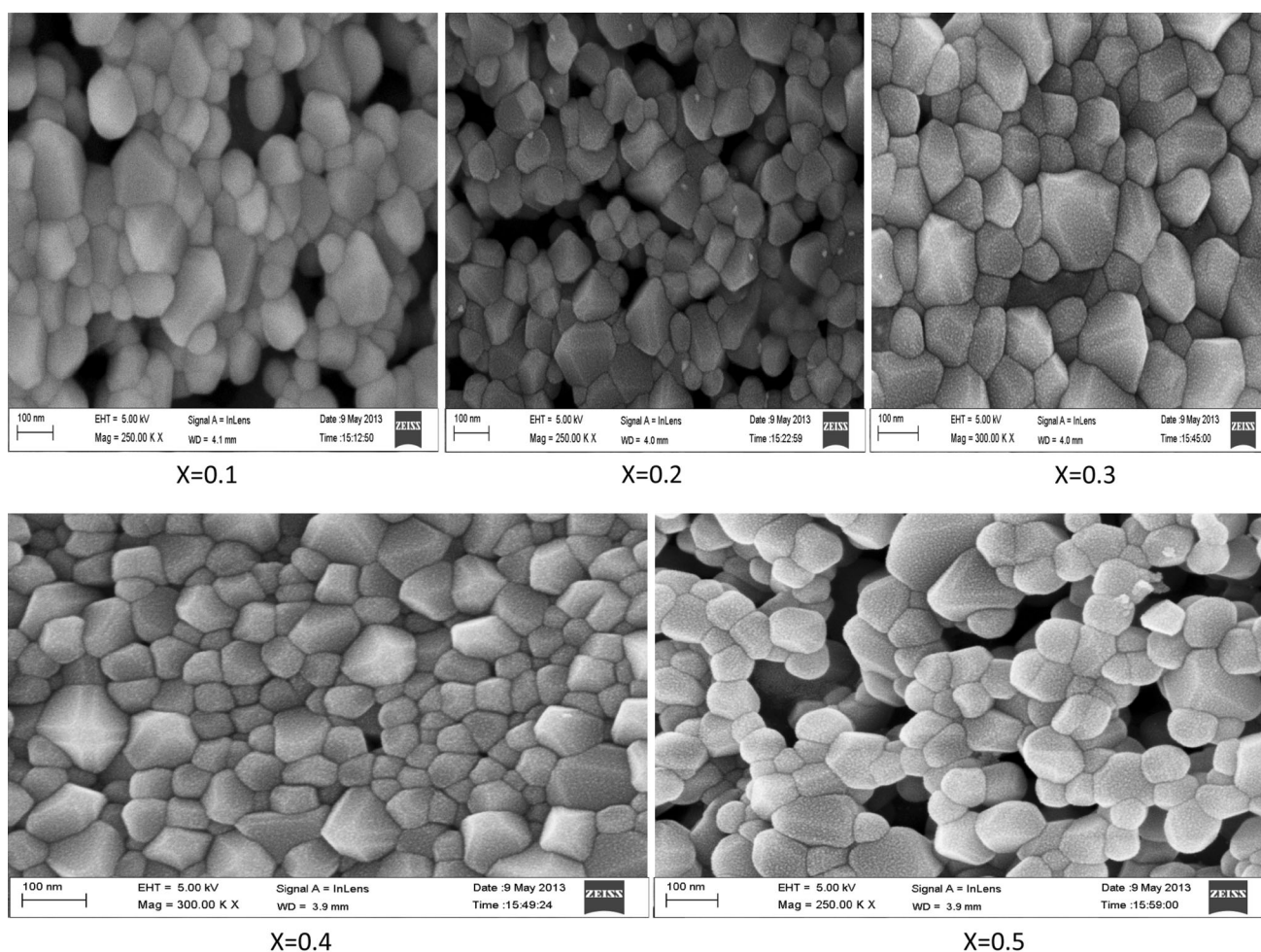
Fig. 4 SEM images of $Cr_x Zn Fe_{2-x} O_4$ samples

planes. This value agrees well with 2.51 Å determined from the analysis of the XRD pattern.

The reason for performing EDAX characterization was to ratify the purity and surety of the chemical composition. A representative energy-dispersive X-ray analysis (EDAX) pattern of $Cr_x Zn Fe_{2-x} O_4$ ($x = 0.3$) is shown in Fig. 5d. The energy-dispersive pattern reflects that these nanoparticles are well crystallized. The EDAX spectrum revealed that the darker particles contain Zn, Cr, Fe, and O as the major elements in the material premeditated with the nonattendance of any impurities. EDAX results suggest that the precursors have fully undergone chemical reaction to form the expected ferrite composition.

M–H loop analysis

The shape and the width of the hysteresis loop depend on the factors such as the chemical composition of the compound, porosity, grain size, etc. The hysteresis loops for the samples have been plotted using vibrating sample magnetometer (VSM) at a maximum field of 15 KG, as shown in Fig. 6a. The various magnetic properties of these samples are listed in Table 4. All the samples exhibit an excellent soft magnetic behavior. The magnetization rises linearly as the applied field increases from zero in either direction and saturation in hysteresis loop was not attained which may be anticipated from the presence of non-magnetic Zn^{2+} ions and low magnetic Cr^{3+} ions in the compound [25]. According to Neel's two-sublattice model, there are three kinds of super-exchange interactions in spinel ferrite, i.e., A–A, B–B, and A–B interactions. The A–B interaction strength is larger than those of A–A and B–B. The net magnetic moment $M = M_B - M_A$ and the large value of M results in higher saturation magnetization. Initially Zn ferrite ($x = 0.0$) shows maximum magnetization of 0.934 emu/g. Whenever Chromium is doped into the sample (at $x = 0.1$), the maximum magnetization is abruptly dropped from 0.934 to 0.376 emu/g. The substitution of low magnetic Cr^{3+} ions (3 μB) replacing the
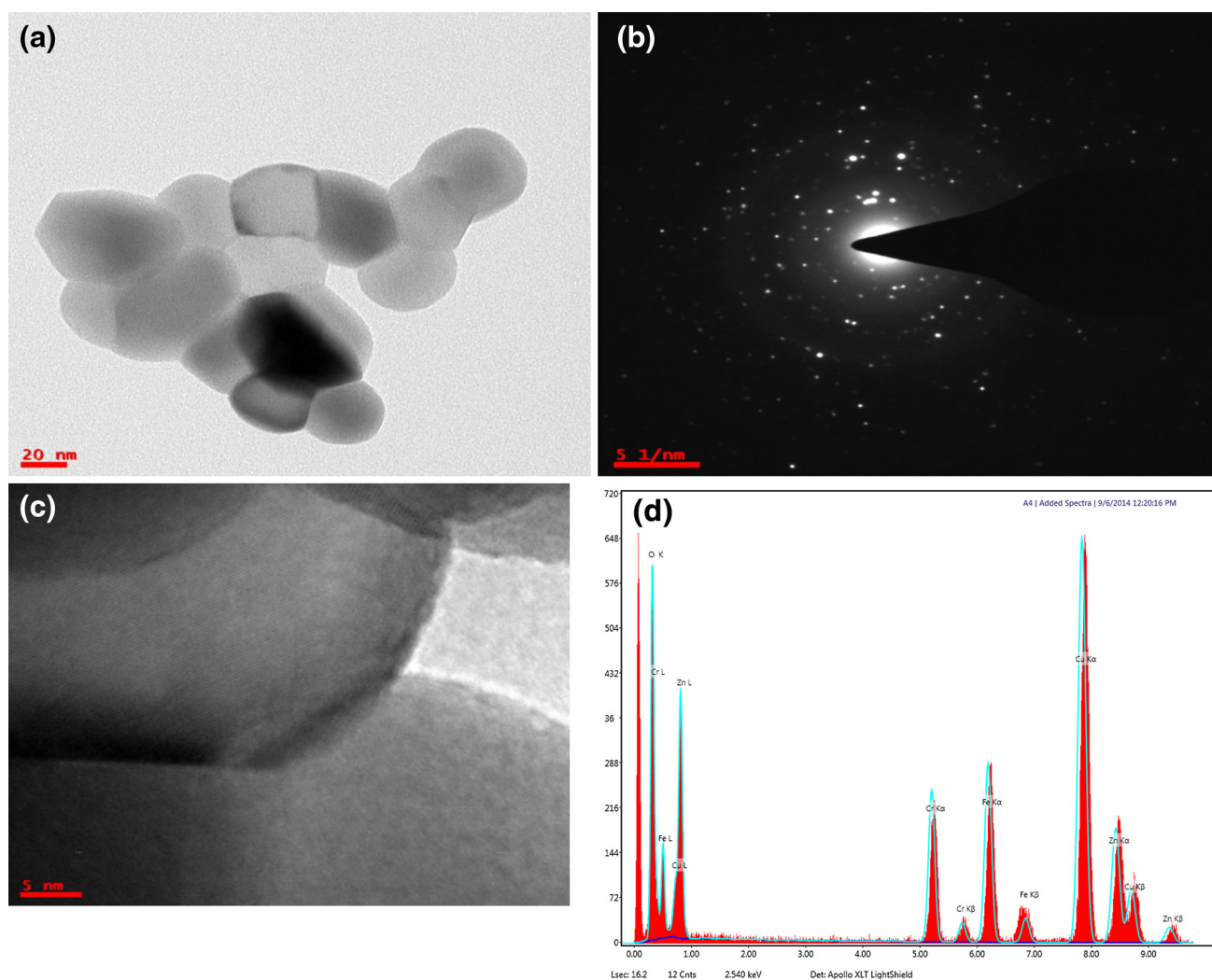
Fig. 5 **a–d** TEM images of $Cr_x Zn Fe_{2-x} O_4$ ($x = 0.3$) sample. **a** TEM micrograph of $Cr_x Zn Fe_{2-x} O_4$ ($x = 0.3$) sample, **b** corresponding SAED pattern of the sample, **c** HRTEM image, and **d** EDAX spectrum

comparatively high magnetic Fe^{3+} ions (5 μB) in B-site might have affected the exchange interaction between A-site and B-site, leading to the decrease in the value of maximum magnetization and thereafter it is increasing steadily with increasing Cr concentration as shown in Fig. 6b. The presence of Zn in the ferrite sample is found to produce spin canting which is responsible for this nonlinearity in magnetization values [26].

In this present study, the sample having a content $x = 0.3$ has the minimum coercivity value of 4.11G. The low coercivity value indicates that the particle can be easily magnetized without any flux loss. The variation of hysteresis loop shape with Cr concentration can be a useful factor. This significant property allows this type of ferrites to be used in the fabrication of magnetic storage media, microwave devices, humidity sensors, magnetic field sensors, transformer cores, etc.

The nano-magnetic particles have special properties as compared to the bulk because of the large volume fraction that atoms occupy at the grain boundary area, which in turn is responsible for several unusual properties like spin canting, surface anisotropy, super paramagnetism (SP), dislocations, etc. [27]. As Chromium concentration increases, the particle size is decreasing and the surface area is increasing. The finite size effect of the nanoparticles leads to a noncollinearity of magnetic moments on their surface, which in turn causes spin disorder [28]. The spin disorder is more when the surface-to-volume ratio is large. Under these circumstances, it is concluded that the interplay of these three interactions, namely super-exchange interaction, magnetocrystalline anisotropy, and canting effect, is more prevalently present in the nanoparticles of ferrite, and hence the magnetic property observed in the system of nanoferrites is a cumulative effect of these interactions.

Fig. 6 a M–H curves for Cr_x Zn Fe_{2-x} O_4 with x = 0.0(A1), 0.1(A2), 0.2(A3), 0.3(A4), 0.4(A5), and 0.5(A6) samples. **b** Variation of maximum magnetization with Cr concentration (x)
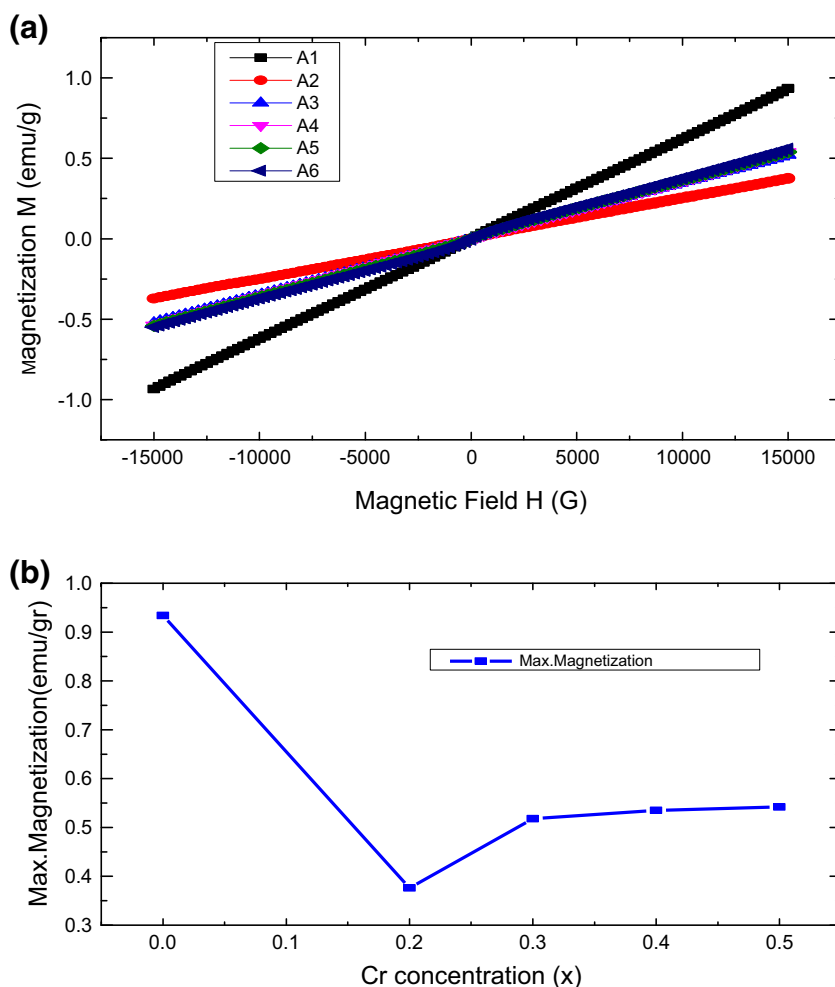

Table 4 Magnetic parameters of Cr_x Zn Fe_{2-x} O_4 (x = 0.0–0.5)

S. no	Cr content (x)	Coercivity (G)	Retentivity (emu/g)	Maximum magnetization (emu/g)
1	$x = 0.0$	20.441	0.00143	0.934
2	$x = 0.1$	18.69	0.000685	0.376
3	$x = 0.2$	29.96	0.00128	0.518
4	$x = 0.3$	4.41	0.000156	0.535
5	$x = 0.4$	21.20	0.0011	0.542
6	$x = 0.5$	96.81	0.0061	0.556

Conclusions

Cr-substituted Zn ferrites with the chemical formula Cr_x Zn Fe_{2-x} O_4 (x = 0.0–0.5) were synthesized by sol–gel method. The structural characterization of the powders using XRD, FTIR, SEM, and TEM-EDAX confirmed the formation of nanosize particles with single-phase spinel structure. The crystallite size, lattice constant, and ion jump lengths were reduced with the increase of chromium concentration due to less ionic radii of Cr^{3+}. X-ray density and surface area have been found to increase with the successive addition of Cr^{3+} ions. The magnetic study for the Cr–Zn ferrite samples indicates that all the magnetic parameters show huge variation and also some cases enhance the magnetic property. From the results, it is clear that the increase in the Cr^{3+} concentration gives the significant changes in the structural and magnetic properties of the Zn ferrite system.

References

1. Mahalakshmi, S., SrinivasaManja, K., Nithiyanantham, S.: Electrical properties of nanophase ferrites doped with rare earth ions. J. Supercond. Novel Magn. **27**, 2083–2088 (2014)

2. Kumar, A.M., Varma, M.C., Dube, C.L., Rao, K., Kashyap, S.C.: Development of Ni–Zn nanoferrite core material with improved saturation magnetization and DC resistivity. J. Magn. Magn. Mater. **320**, 1995–2000 (2008)

3. Hwang, Y.: Microwave absorbing properties of NiZn-ferrite synthesized from waste iron oxide catalyst. Mater. Lett. **60**, 3277–3280 (2006)

4. Yan, W., Li, Q., Zhong, H., Zhong, Z.: Characterization and low-temperature sintering of $Ni_{0.5} Zn_{0.5} Fe_2O_4$ nano-powders prepared by refluxing method. Powder Technol. **192**, 23–26 (2009)

5. Iqbal, M.J., Ahmad, Z., Meydan, T., Melikhov, Y.: Physical, electrical and magnetic properties of nano-sized Co–Cr substituted magnesium ferrites. J. Appl. Phys. **111**, 033906 (2012)

6. Srivastava, M., Chaubey, S., Ojha, A.K.: Investigation on size dependent structural and magnetic behavior of nickel ferrite nanoparticles prepared by sol–gel and hydrothermal methods. Mater. Chem. Phys. **118**, 174–180 (2009)

7. Rafferty, A., Gun'ko, Y., Raghavendra, R.: An investigation of co-fired varistor-Ni Zn ferrite multilayers. Mater. Res. Bull. **44**, 747–752 (2009)

8. Wen, M., Li, Q., Li, Y.: Magnetic, electronic and structural properties of $Zn_xFe_{3−x}O_4$. J. Electron Spectrosc. Relat. Phenom. **153**, 65–70 (2006)

9. Hu, P., Pan, D.A., Wang, X.F., Tian, J.J., Wang, J., Zhang, S.G., Volinsky, A.A.: Fuel additives and heat treatment effects on nanocrystalline zinc ferrite phase composition. J. Magn. Magn. Mater. **323**, 569–573 (2011)

10. Xu, Y., Liang, Y., Jiang, L., Wu, H., Zhao, H., Xue, D.: Preparation and magnetic properties of $ZnFe_2O_4$ nanotubes. J. Nanomater. **2011**, 1–5 (2010)

11. Niederberger, M.: Nonaqueous sol–gel routes to metal oxide nanoparticles. Acc. Chem. Res. **40**, 793–800 (2007)

12. Vijaya kumar, K., Lakshmi, M., Buchi Suresh, M.: Structure-property correlation of sol–gel processed $Co_{0.5} Ti_{0.5} Zn FeO_4$. Int. J. Eng. Res. Ind. Appl. **3**, 1489–1497 (2013)

13. Elahi, A., Ahmad, M., Ali, I., Rana, M.: Preparation and properties of sol–gel synthesized Mg-substituted Ni 2 Y hexagonal ferrites. Ceram. Int. **39**, 983–990 (2013)

14. Haralkar, S., More, S., Shirsath, S.E., Kadam, R., Mane, D.: Ion jump lengths of Mn–Zn–Al–Fe And Mg–Zn–Cr–Fe nano-particles. Ind. Str. Res. J. **2**, 1–6 (2012)

15. Gunjal, R., Kakade, G., Jadhav, K.: Dielectric properties of chromium substituted manganese ferrites. Int. J. Adhes. Advan. Eng. Tech. **3**, 16–17 (2012)

16. Kumar, A., Yadav, K.: Magnetic, magnetocapacitance and dielectric properties of Cr doped bismuth ferrite nanoceramics. Mater. Sci. Eng. B **176**, 227–230 (2011)

17. Rahman, M.M., Sheak, M.S., Pervin, S., Uddin, N., Ahmed, F., Hossain, M.A., Rahaman, M., Bashar, M.S., Hossain, T., Akhter, S.: Composition, temperature and frequency dependent magnetic, dielectric and electrical properties of magnesium–zinc ferrites. J. Bangladesh Acad. Sci. **36**, 199–212 (2012)

18. Haralkar, S., Kadam, R., More, S., Shirsath, S.E., Mane, M., Patil, S., Mane, D.: Substitutional effect of Cr^{3+} ions on the properties of Mg–Zn ferrite nanoparticles. Phys. B **407**, 4338–4346 (2012)

19. Mustafa, G., Islam, M., Zhang, W., Jamil, Y., Anwar, A.W., Hussain, M., Ahmad, M.: Investigation of structural and magnetic properties of Ce^{3+}-substituted nanosized Co–Cr ferrites for a variety of applications. J. Alloys Compd. **618**, 428–436 (2015)

20. Hashim, M., Shirsath, S.E., Kumar, S., Kumar, R., Roy, A.S., Shah, J., Kotnala, R.: Preparation and characterization chemistry of nano-crystalline Ni–Cu–Zn ferrite. J. Alloys Compd. **549**, 348–357 (2013)

21. Waldron, R.: Infrared spectra of ferrites. Phys. Rev. **99**, 1727 (1955)

22. Sutka, A., Mezinskis, G., Pludons, A., Lagzdina, S.: Characterization of solgel auto-combustion derived spinel ferrite nano-materials. Power Eng. **56**, 254–259 (2010)

23. El-Sayed, A.: Effect of chromium substitutions on some properties of NiZn ferrites. Ceram. Int. **28**, 651–655 (2002)

24. Hankare, P., Patil, R., Jadhav, A., Pandav, R., Garadkar, K., Sasikala, R., Tripathi, A.: Synthesis and characterization of nanocrystalline Ti-substituted Zn ferrite. J. Alloys Compd. **509**, 2160–2163 (2011)

25. Bahadur, D., Rajakumar, S., Kumar, A.: Influence of fuel ratios on auto combustion synthesis of barium ferrite nano particles. J. Chem. Sci. **118**, 15–21 (2006)

26. Jadhav, S.S., Gore, S., Patange, S., Shirsath, S.: Effect of Cr ions on physical properties of Cu–Zn ferrite nano-particles. Inter. J. Basic Appl. Res. 78–81 (2012)

27. Ghasemi, A., Ekhlasi, S., Mousavinia, M.: Effect of Cr and Al substitution cations on the structural and magnetic properties of $Ni_{0.6} Zn_{0.4} Fe_{2−x} Cr_{x/2} Al_{x/2} O_4$ nanoparticles synthesized using the sol–gel auto-combustion method. J. Magn. Magn. Mater. **354**, 136–145 (2014)

28. Masti, S., Sharma, A., Vasambekar, P., Vaingankar, A.: Influence of Cd^{2+} and Cr^{3+} substitutions on the magnetization and permeability of magnesium ferrites. J. Magn. Magn. Mater. **305**, 436–439 (2006)